frontiers | Frontiers in Bioengineering and Biotechnology

TYPE Original Research
PUBLISHED 22 February 2024
DOI 10.3389/fbioe.2024.1276143

OPEN ACCESS

EDITED BY
Salavat Aglyamov,
University of Houston, United States

REVIEWED BY
Ilya Pyatnitskiy,
The University of Texas at Austin, United States
Jinmo Jeong,
The University of Texas at Austin, United States

*CORRESPONDENCE
Massoud L. Khraiche,
mkhraiche@aub.edu.lb

RECEIVED 11 August 2023
ACCEPTED 06 February 2024
PUBLISHED 22 February 2024

CITATION
Badawe HM, Raad P and Khraiche ML (2024), High-resolution acoustic mapping of tunable gelatin-based phantoms for ultrasound tissue characterization.
Front. Bioeng. Biotechnol. 12:1276143.
doi: 10.3389/fbioe.2024.1276143

High-resolution acoustic mapping of tunable gelatin-based phantoms for ultrasound tissue characterization

Heba M. Badawe, Petra Raad and Massoud L. Khraiche*

Neural Engineering and Nanobiosensors Group, Biomedical Engineering Program, Maroun Semaan Faculty of Engineering and Architecture, American University of Beirut, Beirut, Lebanon

Background: The choice of gelatin as the phantom material is underpinned by several key advantages it offers over other materials in the context of ultrasonic applications. Gelatin exhibits spatial and temporal uniformity, which is essential in creating reliable tissue-mimicking phantoms. Its stability ensures that the phantom's properties remain consistent over time, while its flexibility allows for customization to match the acoustic characteristics of specific tissues, in addition to its low levels of ultrasound scattering. These attributes collectively make gelatin a preferred choice for fabricating phantoms in ultrasound-related research.

Methods: We developed gelatin-based phantoms with adjustable parameters and conducted high-resolution measurements of ultrasound wave attenuation when interacting with the gelatin phantoms. We utilized a motorized acoustic system designed for 3D acoustic mapping. Mechanical evaluation of phantom elasticity was performed using unconfined compression tests. We particularly examined how varying gelatin concentration influenced ultrasound maximal intensity and subsequent acoustic attenuation across the acoustic profile. To validate our findings, we conducted computational simulations to compare our data with predicted acoustic outcomes.

Results: Our results demonstrated high-resolution mapping of ultrasound waves in both gelatin-based phantoms and plain fluid environments. Following an increase in the gelatin concentration, the maximum intensity dropped by 30% and 48% with the 5 MHz and 1 MHz frequencies respectively, while the attenuation coefficient increased, with 67% more attenuation at the 1 MHz frequency recorded at the highest concentration. The size of the focal areas increased systematically as a function of increasing applied voltage and duty cycle yet decreased as a function of increased ultrasonic frequency. Simulation results verified the experimental results with less than 10% deviation.

Conclusion: We developed gelatin-based ultrasound phantoms as a reliable and reproducible tool for examining the acoustic and mechanical attenuations taking place as a function of increased tissue elasticity and stiffness. Our experimental measurements and simulations gave insight into the potential use of such phantoms for mimicking soft tissue properties.

KEYWORDS

tissue mimicking phantom, ultrasound, mechanical properties, acoustic properties, intensity attenuation

1 Introduction

Ultrasound is a non-invasive modality used clinically for diagnostic and therapeutic purposes (Escoffre and Bouakaz, 2015). Ultrasonic beams can be focused on target tissues with high spatial and temporal resolution overcoming, to a certain extent, tissue inhomogeneity (Polanía et al., 2018). Ultrasound has a wide range of applications, including both diagnosis and treatment with the latter depending on the intensity and frequency used (Baek et al., 2017). For instance, low-intensity focused ultrasound (LIFUS) has demonstrated neuromodulation capabilities, enabling the reversible excitation or inhibition of neurons with no reported brain damage (Khraiche et al., 2008; El Hassan et al., 2022), whereas high intensity focused ultrasound (HIFU) causes lesions and ablates cancerous tumors irreversibly (Khraiche et al., 2009; Maloney and Hwang, 2015), depending on the exposure time and tissue temperature elevation, thus becoming a potential neurosurgery technique. Besides neuromodulation, ultrasound is mainly used in image-guided tissue visualization in pre-clinical and clinical applications, allowing treatment planning and online assessment of ultrasound interactions with target tissues (Ebbini and Ter Haar, 2015). Even though ultrasonic imaging has some limitations in the overall showcasing of tissue anatomy, it provides valuable information on tissue dynamics, blood flow, and soft tissue stiffness and elasticity (Wells and Liang, 2011).

Applying ultrasound waves to spatially and temporally uniform tissue-mimicking phantoms can aid in understanding the amount of beam distortion and attenuation taking place throughout the whole volume (Kim et al., 2012). Constructing a phantom that mimics the acoustic, optical, electrical, thermal, and mechanical properties of biological tissues can be crucial for pre-clinical and clinical applications of ultrasound (Cook et al., 2011; Khraiche et al., 2013). A tissue phantom can be homogeneous or heterogeneous, mimicking the various layers of tissue in question. Yuan et al. constructed a phantom representing the human thigh with an embedded tumor enclosing the fat, muscles, and bones (Yuan et al., 2012). Li et al. formulated a composition of different oils and chemical materials to represent the breasts and surrounding tissues in an attempt to study the interactions between such materials with ultrasound and microwave radiations (Kamimura et al., 2021).

Tuning the various tissue properties is feasible during the design and fabrication stage through different chemical additives and mechanical compositions to account for the different geometrical shapes of the target tissues (Chen et al., 2016). Even for medical practices and surgical purposes, silicone-based phantoms were constructed to assess the flexibility, accuracy, and functionality of medical tools (Wang et al., 2014). In the thermal ablation field, ultrasound or magnetic resonance imaging modalities can be guided by the tumor phantom inserted within the normal tissue phantom for targeted ablation based on tumor color change at higher temperatures (Negussie et al., 2016; Zhong et al., 2022). Takagi et al. developed a color-coded, thermochromic liquid-crystal tissue-mimicking phantom, composed of two layers with different temperature sensitivity ranges, for better visualization of the distribution of high-intensity focused ultrasound waves around the focal point (Takagi et al., 2022). High-intensity ultrasound attenuation can also be detected based on the tissue displacement induced within the phantom in the direction of the ultrasound beam and can be visualized through ultrasound imaging (Kamimura et al., 2021). Biomechanical characterization of a tissue-mimicking phantom involves identifying its acoustic and mechanical properties. Acoustic measurements for the speed of sound and attenuation coefficient can be performed using the through-transmission technique, while the elastic properties can be evaluated from ultrasound sheer wave speed maps or through compression tests to identify Young's modulus (Hofstetter et al., 2020).

Many studies document the use of different types of chemicals to prepare mechanically identical tissue-mimicking phantoms including water-based phantoms. Polyvinyl alcohol (PVA) cryogel demonstrated adjustable mechanical properties when exposed to freeze-thaw techniques for intravascular elastography (Chu and Rutt, 1997; Fromageau et al., 2003; Minton et al., 2012). Polyacrylamide gels have also been used to fabricate tissue-mimicking phantoms with better physical stability than other water-based phantoms (Kawabata et al., 2004; Kumar et al., 2010; Khraiche and El Hassan, 2020). In addition, agarose-based phantom materials are used in some studies due to their biocompatibility and mechanobiological resemblance to various biological tissues (Zarrintaj et al., 2018). However, gelatin is regarded as one of the most flexible materials to work with, providing controllable parameters for a rapid and inexpensive recipe for phantom formation. Gelatin records stable elasticity levels and geometry after forming (Madsen et al., 2006). As for its ultrasonic characterizations, gelatin allows limited scattering levels of ultrasound beams (Hofstetter et al., 2020).

In this work, we build high-resolution acoustic maps of ultrasound waves propagating in water, to study the effect of ultrasound frequency, duty cycle, and voltage on the maximal acoustic intensity and area of the focal region. We then develop gelatin-based phantoms, with three different gelatin concentrations that represent various soft tissues with similar mechanical, and acoustic characteristics, to account for the attenuation in the maximal acoustic intensity. After that, we study the effect of increasing gelatin concentration on the compressive stress and strain and the mean Young's modulus of the gelatin-based phantoms. According to the desired acoustic and mechanical properties needed for any specific application, the user can determine the right recipe for mimicking their biological tissue at hand, with their corresponding acoustic attenuation and mechanical elasticity.

2 Materials and methods

2.1 Experimental setup

A motorized system was assembled as in Figure 1 to map the acoustic profile of the ultrasound transducer at 30 μm resolution and generate heat maps that illustrate the transfer of intensity of ultrasound waves in a specific volume of water. This helped characterize the acoustic intensity at the focal region while using three different drive voltages of 110 mV, 120 mV, and 165 mV, with transducers of three different frequencies of 1 MHz, 5 MHz, and 7.5 MHz. Following that, and to characterize the effect of gelatin-based phantoms with three different gelatin concentrations on the

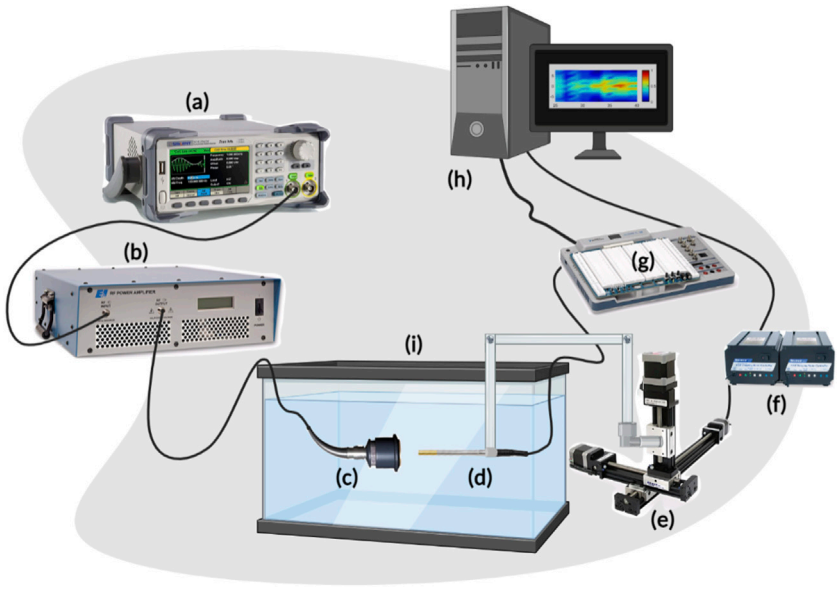

FIGURE 1
Scheme of the acoustic profile set-up. **(A)** represents the function generator producing a pulsed sine wave. **(B)** is the RF power amplifier which amplifies the sinusoidal RF signal that is converted to ultrasonic pressure waves by the ultrasound transducer **(C)**. The hydrophone **(D)** is driven by the 3-D motorized system **(E)**, powered by the VXM stepping motor controller **(F)**, and converts the mechanical signals received from the transducer into electrical signals while scanning a 3D volume in front of the face of the transducer. The voltage signals from the hydrophone are received by the Elvis III data acquisition board (DAQ) **(G)** and relayed back to the PC **(H)** for further processing. Both the transducer and hydrophone are submerged in the degassed water tank **(I)** of dimensions 40 cm × 20 cm × 16 cm.

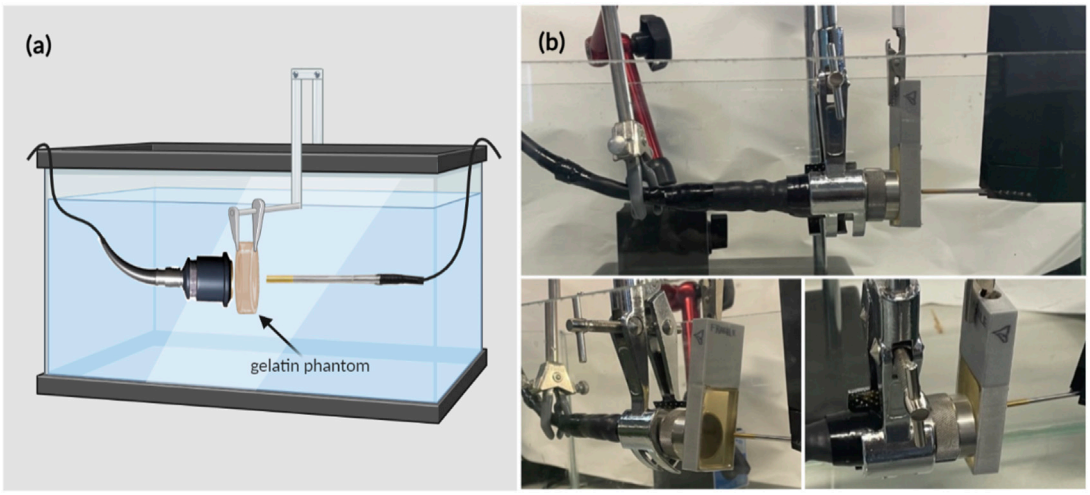

FIGURE 2
Experimental setup for estimating the acoustic intensity and attenuation coefficient when the gelatin phantoms, of different concentrations, were introduced. **(A)** Schematic diagram of the experimental setup including the gelatin phantom in place in front of the face of the transducer. **(B)** Real-time images showing the ultrasonic signal acquisition setup arrangement, from different views, in which the phantom was held (by the rectangular phantom holder) between the transducer and the hydrophone.

acoustic intensity and attenuation, the horizontal planes facing the transducer were scanned; the gelatin-based phantoms were positioned between the transducer probe and hydrophone, adjacent to the transducer face (Figure 2).

The schematic in Figure 1 describes the acoustic setup built for obtaining the acoustic profiles and the acoustic characterization of the gelatin-based phantoms with all the required connections. The pulsed ultrasonic waves were generated from the 2-channel Siglent arbitrary waveform generator (SDG 2042X; maximum output = 40 MHz; maximum sampling rate = 1.2GSa/s; 50 Ω impedance) to which a 50-dB-gain radio frequency (RF) power amplifier was connected (Electronics and Innovation, Rochester New York

TABLE 1 Properties of the focused transducers used in the experiments.

Manufacturer	Frequency (MHz)	Focal length (mm)	Center frequency (MHz)	Peak frequency (MHz)	(-6) dB bandwidth (%)
Olympus	1.00	37.19	0.96	1.04	73.35
Olympus	5.00	39.52	4.77	4.86	66.52
Olympus	7.50	36.39	6.76	7.26	83.95

14,623; 1.0 V_{rms} input; 50 Ω input/output impedance). RF signals from the generator were amplified by the RF power amplifier, before being transmitted through a single-element, focused ultrasonic transducer. In general, three focused transducers were used in the experiments with their properties provided in Table 1. The outer diameter of the transducers is 19.05 mm and can be submerged in degassed water for up to 8 h, long enough for the experiment to be conducted, followed by a dry time of 16 h to ensure a proper lifetime of the unit. Furthermore, an immersible needle hydrophone (Onda HNR-0500) of size 37.3 mm × 2.5 mm was controlled by a 3D-axis motorized system programmed with a LabView sub-VI to scan a predetermined volume, then quantize and convert the sound pressure waves emitted by the transducer while traveling through the water tank into voltage signals by the piezoelectric effect. The hydrophone has an operating frequency range of 0.25 MHz–10 MHz, a maximum operating temperature of 50°C, a capacitance of 200 pF, and an end-of-cable nominal sensitivity of 0.126 V/MPa. Through the data acquisition board (Elvis III, National Instruments; input voltage ≤50 V DC, or 30 V_{rms}) connected to the hydrophone, the ultrasonic pressure signals were stored as voltage signals, and measured over lateral and longitudinal planes of the ultrasound focal region.

The acquired voltage signals were processed and analyzed offline through an in-house MATLAB code, and the spatial-peak pulse-average intensity (I_{SPPA}) was evaluated based on Equations 1–5 presented in the section "Acoustic measurements". The ultrasonic voltage data were acquired in water only (Figure 1) and with the phantom placed in between the transducer and the hydrophone (Figure 2). The attenuation coefficient (experimental value) of the phantom was thereafter calculated from these data sets using equation (S5).

For the mechanical assessment of Young's modulus of the gelatin-based phantoms, compression tests, using the Universal Testing Machine (825 University Ave, Norwood, MA, US), were conducted on ten cylindrical specimens of various gelatin concentrations to calculate the mean modulus of elasticity. Each sample of the cylindrical phantom of a particular concentration was placed on a 10-N load cell to be compressed. The aim was to study the effect of increasing phantom gelatin concentration on the elasticity modulus mimicking certain soft biological tissues.

2.2 Phantom recipe and modeling

The gelatin-based phantoms were prepared using commercially available, low-cost, plant-based gelatin (Sigma-Aldrich). First, 10 mL of osmosed water was preheated to 60°C in a beaker placed on a hot plate. The gelatin powder was then gradually added to the beaker (in amounts depending on the gelatin concentration needed) and constantly stirred with a magnetic stirrer until totally dissolved. Air bubbles were removed using a fine spatula to eliminate undesirable experimental distortions (Dahmani et al., 2019). The mixture was then poured into a 3D-printed rectangular mold (40 mm by 25 mm) that was previously lightly coated with oil to help in the unmolding process following refrigeration. The mold was then transferred to a refrigerator for 24 h to obtain firm enough phantoms that could withstand long hours of being submerged in water. Note that the mold was preserved in a covered petri dish to prevent dehydration of the surface. To investigate the effect of gelatin concentration on the acoustic attenuation, different phantoms of respective gelatin concentrations (12.5%, 20%, and 24%) were prepared, where x % corresponds to x grams of gelatin powder poured in 100 mL of water. Following the 24 h of refrigeration, the phantoms were removed from the fridge, unmolded, and mounted in our setup (Figure 2).

2.3 Mechanical measurements

To test the mechanical properties of phantoms with increasing gelatin concentrations, samples of respective gelatin concentrations of 12.5%, 20%, and 24% were prepared. When removed from the fridge and unmolded, ten cylindrical specimens of an average height of 8 mm and 5 mm diameter were directly cut from each gelatin-based phantom (of a particular concentration) for mechanical testing. Compression tests were performed on each cylindrical specimen at a displacement rate of 0.1 mm/s up to a maximum strain of 0.4 mm/mm using the Instron machine. At room temperature, each specimen was placed on the compression plate with a preload of 0.1 N set for the upper plate to precisely get in contact with the specimen. The stress and strain of each specimen were estimated using the testing machine's built-in software (Bluehill Universal 3.0), and the mean Young's modulus was calculated and plotted as a function of gelatin concentration.

2.4 Acoustic measurements

The motorized setup used LabView VI for system control and data acquisition. The acquired voltage measurements underwent filtering to clean the signal from any noise, and the acoustic intensity of ultrasonic waves was calculated from the filtered voltage matrix according to the guidelines of the Food and Drug Administration (Food and Drug Administration, 2008). For the computations, the following pipeline was followed: First, the pulse intensity integral

(PII) was computed, defined as the time integral of instantaneous intensity integrated over the time in which the hydrophone signal for the specific pulse was nonzero. The instantaneous acoustic intensity i is expressed as:

$$i = \frac{p^2(t)}{\rho c} \tag{1}$$

where $p(t)$ is the instantaneous acoustic pressure, ρ is the density of the medium, and c is the speed of sound in the medium (all in SI units). The pressure p is expressed as:

$$p(t) = \frac{v(t)}{M} \tag{2}$$

where $v(t)$ is the acquired voltage array that varies with the position of the hydrophone with respect to the transducer, and M is the end-of-cable nominal sensitivity of the hydrophone. Thus, PII is expressed as:

$$PII = \frac{\int_{t_1}^{t_2} p^2(t)dt}{\rho c} = \frac{\int_{t_1}^{t_2} v^2(t)dt}{\rho c \cdot M^2} \tag{3}$$

where $(t_2 - t_1)$ is the interval in which the amplitude of the recorded voltage is nonzero (i.e., $t_2 - t_1$ = tone-burst-duration). PII corresponds to the energy transferred per unit area (expressed in J/m^2) or the energy fluence during one pulse. Following that, the pulse duration (PD) was calculated, defined as:

$$PD = 1.25(t_3 - t_4) \tag{4}$$

t_4 is the time instant at which the time integral of intensity reaches 90% of PII, and t_3 is the instant at which the time integral reaches 10% of PII. Finally, the spatial-peak pulse-average intensity (I_{SPPA}) was calculated as the maximum ratio of PII (energy fluence per pulse) to PD:

$$I_{SPPA} = \frac{PII}{PD} \tag{5}$$

Thus, calculations of the true I_{SPPA} were not obstructed. With the 1 MHz, 5 MHz, and 7.5 MHz transducers, three different voltages (110 mV, 120 mV, and 165 mV) were used to characterize the acoustic profile of ultrasound waves propagating in degassed water, followed by characterizing the effect of gelatin concentration on the acoustic profile with fixed ultrasound frequency and received voltage.

2.5 Acoustic simulations

Simulations were performed using K-wave, an open-source acoustics MATLAB toolbox, used for modeling the propagation of acoustic waves in well-defined media (Treeby and Cox, 2010). The dynamic changes that an acoustic wave undergoes while passing through a 2D compressible medium are expressed with partial differential equations, solved using a k-space pseudo-spectral method. Computations were performed in a 64 by 128 computational grid with a step size of 0.3 mm, enveloped with a perfectly matched layer, occupying 20 grid points covering the circumference of the domain to prevent reflection and wave wrapping. The ultrasound transducer was modeled as a spherically focused acoustic source driven at a frequency of 1 MHz and emitting acoustic waves that were focused on a definitive distance of 36 mm from the face of the transducer.

Simulations were carried out in four different settings: acoustic waves propagating in a homogeneous medium containing degassed water only, and heterogeneous media where a gelatin phantom, of three different gelatin concentrations (12.5%, 20%, and 24%), was positioned in direct contact with the face of the transducer. Medium properties (sound speed, density, and acoustic absorption coefficient) defining the simulations of water and phantoms of different gelatin concentrations are described in Supplementary Table S1, such that values were obtained based on the study of Chen et al. (Chen et al., 2016). A sensor mask was designed as in Supplementary Figure S1 to record the acoustic field at each time step while the acoustic waves propagated through the gelatin phantom and water respectively, taking into consideration the medium properties as they were systematically defined in a piecewise fashion according to the phantom geometry. Calculations of the attenuation coefficient α are detailed in the supplementary based on the studies of (Prince and Links, 2006; Mahesh, 2013).

3 Results

3.1 Effect of frequency, voltage, and duty cycle on acoustic profile and intensity

To characterize the propagation of ultrasonic waves in water, three transducers were used. Whereby the variation of the acoustic profile and the variation of intensity distribution across the horizontal midplane (the center horizontal plane perpendicular to the transducer's face) and vertical transverse sections of the ultrasound beam were studied with the 1 MHz, 5 MHz, and 7.5 MHz transducers while increasing the applied voltage (110 mV, 120 mV, and 165 mV), and keeping a constant duty cycle of 100 cycles per pulse (Figures 3–5). As the ultrasound beams propagated in water, in the x direction, to reach the maximal intensity at the focal point, the size of the horizontal and vertical focal areas increased systematically as a function of increasing applied voltage yet dropped as a function of increased ultrasonic frequency (Figures 7A,B). Note that the horizontal area corresponds to the area of the horizontal midplane, and the vertical area measures the area at the vertical cross-section near the focal point and at the focal point, with a cutoff threshold of 85% (inclusive) of the computed maximum intensity. The wider focal area was recorded using the 1 MHz transducer at the highest voltage applied of 165 mV. The higher the voltage and frequency used, the higher the maximal intensity at the focal point reached (Figure 7C).

Regarding the effect of varying the duty cycle on the acoustic profile in general and the maximal intensity at the focal point, the 5 MHz transducer was used while receiving a voltage of 120 mV. Incrementing the duty cycle from 33% to 44%, followed by 67%, caused respective 27% and 36.7% increases in the maximal intensity (Figure 7D). Yet the acoustic profile showed a similar intensity spread with all duty cycles used (Figure 6), whereby the horizontal and vertical areas of the focal region demonstrated an insignificant change.

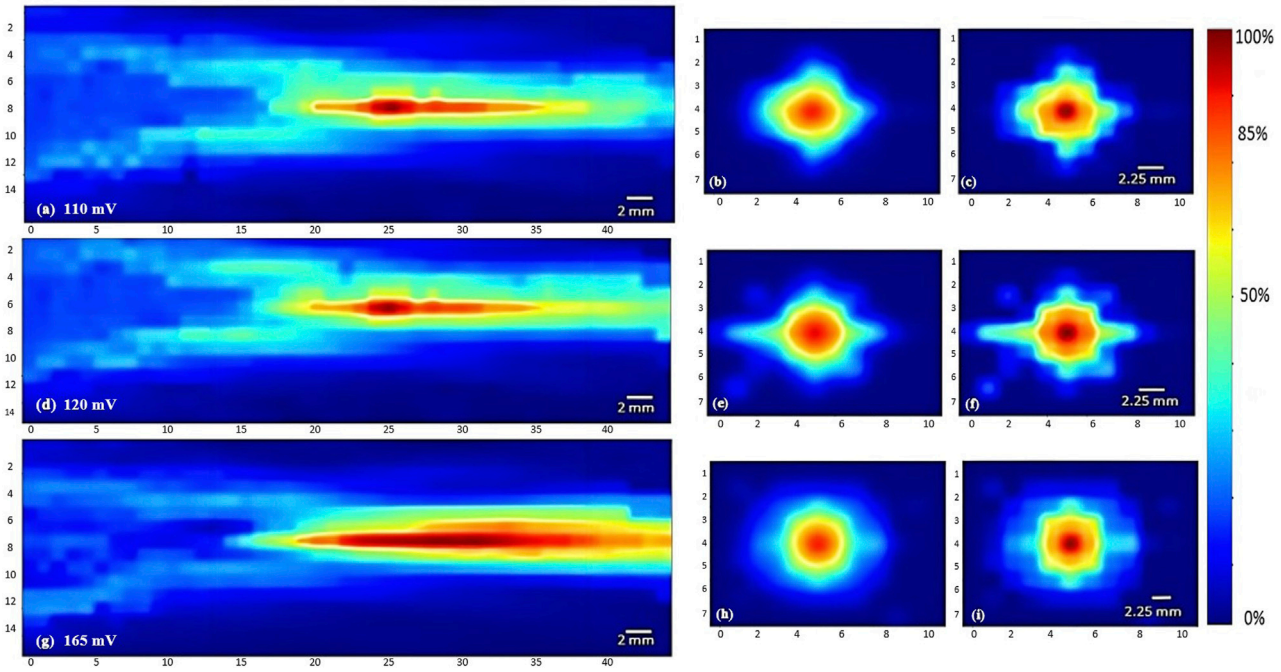

FIGURE 3
Heat maps of the intensity distribution (with respect to the maximal intensity) using the 1 MHz transducer. The horizontal midplane, vertical plane - transverse section near the focal point and at the focal point plotted respectively with a voltage of 110 mV **(A,B,C)**, a voltage of 120 mV **(D,E,F)**, and a voltage of 165 mV **(G,H,I)**.

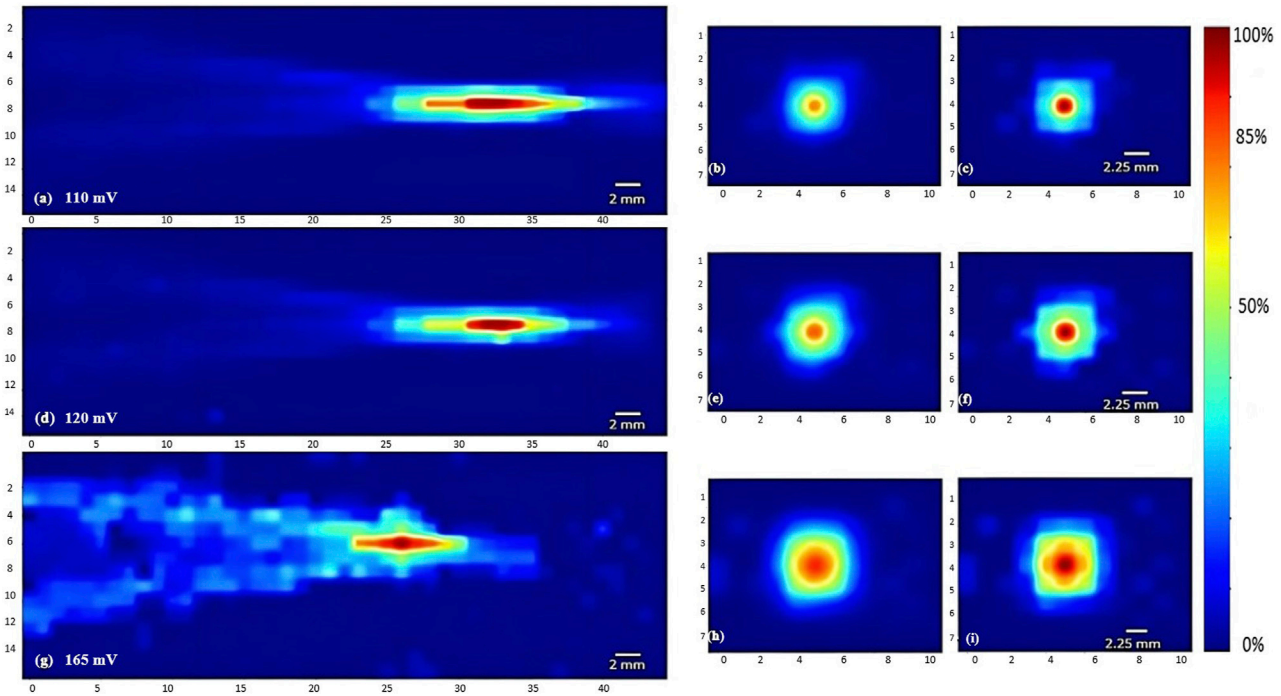

FIGURE 4
Heat maps of the intensity distribution (with respect to the maximal intensity) using the 5 MHz transducer. The horizontal midplane, vertical plane - transverse section near the focal point and at the focal point plotted respectively with a voltage of 110 mV **(A,B,C)**, a voltage of 120 mV **(D,E,F)**, and a voltage of 165 mV **(G,H,I)**.

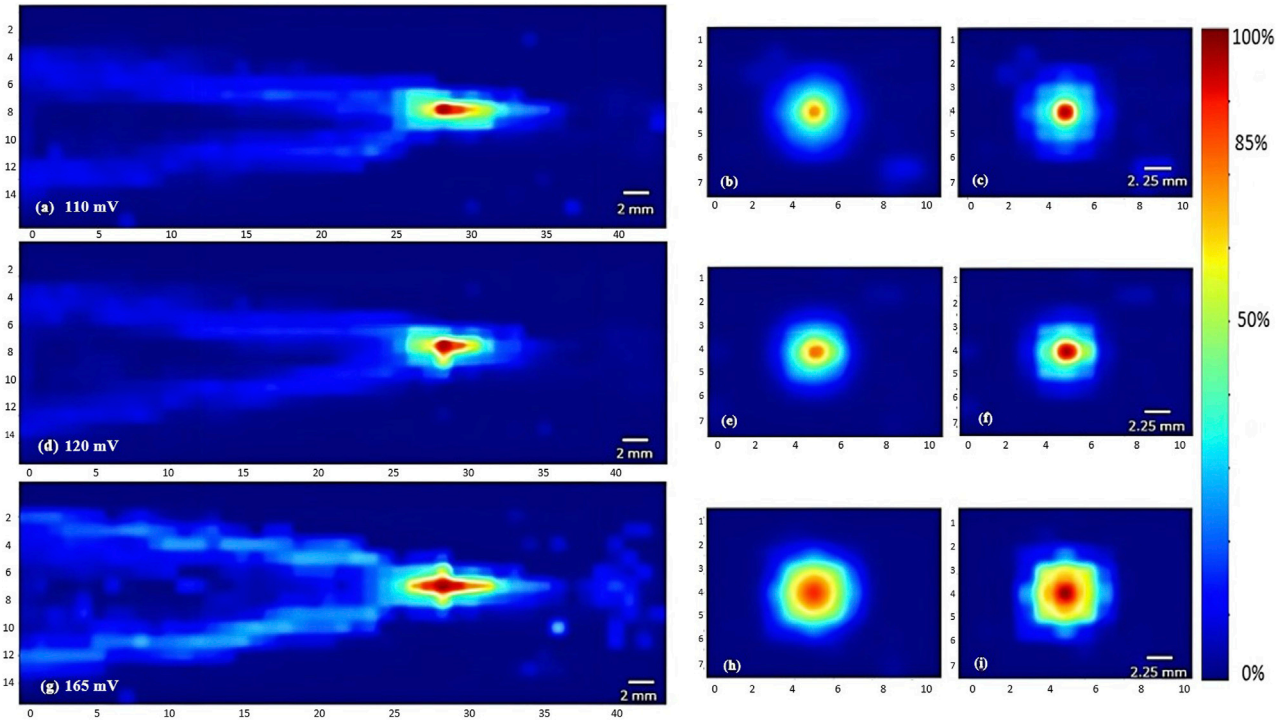

FIGURE 5
Heat maps of the intensity distribution (with respect to the maximal intensity) using the 7.5 MHz transducer. The horizontal midplane, vertical plane - transverse section near the focal point and at the focal point plotted respectively with a voltage of 110 mV **(A,B,C)**, a voltage of 120 mV **(D,E,F)**, and a voltage of 165 mV **(G,H,I)**.

3.2 Acoustic assessment of gelatin-based phantoms

Experimental acoustic characterization of the gelatin-based phantoms was done using our experimental acoustic setup. That same horizontal midplane in front of the face of the transducer was scanned, where all the gelatin-based phantoms of the three different concentrations were placed consecutively. In the first set of experiments, the function generator emitted a signal of 1 MHz fundamental frequency, a burst period of 125 μs (a duty cycle of 80%), and an amplitude of 150 m V_{pp}. The second set of experiments included the 5 MHz transducer, emitting at a burst period of 40 μs and amplitude of 90 m V_{pp}. The maximum I_{SPPA} was computed from the voltage measurements in each experiment, and the attenuation coefficient α was calculated using equation (S5).

Computing the normalized intensity with respect to the maximal intensity recorded at the focal point in both experiments showed a decreasing trend with an increase in the gelatin concentration (Figure 7E). Specifically, a 30% drop was evaluated at the 5 MHz sonication, in comparison with a 48% decrease with the 1 MHz sonication, between the lowest and highest gelatin concentrations studied. Add to that, the 5 MHz transducer recorded higher normalized acoustic intensities at all gelatin concentrations when compared to those of the 1 MHz transducer, recording a 39% increase at the highest gelatin concentration of 24%. On the other hand, the attenuation coefficient increased as more gelatin powder was added with a 67% increase in attenuation at the highest concentration when sonicating at a 1 MHz frequency in comparison with the 5 MHz frequency (Figure 7F).

Adding more gelatin powder to the solution rendered the gelatin-based phantoms more acoustically attenuating where the ultrasound waves emerging from the phantom transferred less power per unit area. The drop in the maximum intensity and subsequent rise in the attenuation coefficient following the increase in gelatin concentration can be visualized in the acoustic scans of Figure 8. The higher the fundamental frequency, the more confined the acoustic profile spread. With the 5 MHz transducer, the focal area, in both the vertical sense and horizontal sense, was narrower than that with the 1 MHz transducer. Add to that, the acoustic impedance characterized as the product of the density of the gelatin-based phantoms with the speed of sound through the phantoms increased as the gelatin concentration increased. Mainly, $Z_{12.5}$ = 1.63 MRayl, Z_{20} = 1.66 MRayl, and Z_{24} = 1.72 MRayl.

3.3 Acoustic profile simulations

We modeled the propagation of ultrasound waves in the media mimicking biological tissues for effective planning and application. The medium properties and geometries determined the acoustic nonlinearity and power absorption for more accurate modeling. Simulations aided in calculating the maximal intensity at the focal point in front of the face of the 1 MHz transducer which approximately scaled with the acoustic fields calculated

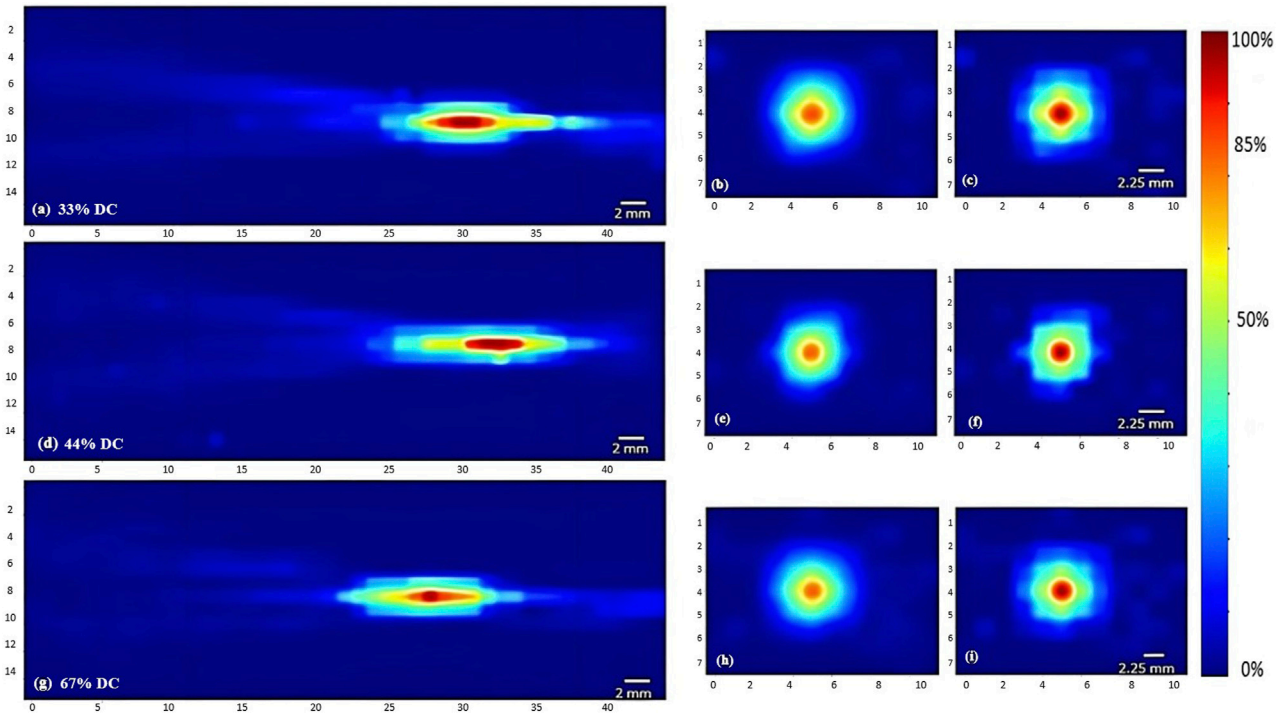

FIGURE 6
Heat maps of the intensity distribution (with respect to the maximal intensity) using the 5 MHz transducer at 120 mV with varying duty cycles. The horizontal midplane, vertical plane - transverse section near the focal point and at the focal point plotted respectively with a duty cycle of 33% **(A,B,C)**, a duty cycle of 44% **(D,E,F)**, and a duty cycle of 67% **(G,H,I)**.

experimentally. The differences between measured and simulated acoustic fields could arise from various experimental changes including equipment properties, signal detection through the mounted hydrophone, and signal processing (Martin et al., 2019). Add to that, the phantom properties from dimensions and thickness to refrigeration time and density, affected the attenuation coefficient measurements as well. Nevertheless, the deviation was within an acceptable range for accurate predictions of a percentage deviation less than 10% (Figure 9A).

In the simulation experiments, the maximum intensity recorded at the focal point dropped as the gelatin concentration increased (Figure 9A). Simulations showed a similar trend as the experimental data, emphasizing the effect of increasing gelatin concentration on the drop of maximal intensity at the focal point. As a result, the higher the gelatin concentration, the higher the acoustic attenuation (Figure 9B). The effect of increasing gelatin concentration could also be detected in the full-volume scans of the acoustic profile in the four settings (Figures 9C–F) where the d, e, and f plots illustrated the drop in the maximum intensity recorded when the different gelatin phantoms were introduced with respect to the maximal intensity of 0.76 W/cm^2 recorded in water only.

3.4 Experimental mechanical measurements

For optimal choice of acoustic parameters, it is crucial to estimate the effect of biological tissues on the intensities of ultrasound waves travelling through them. Consequently, gelatin-based phantoms were prepared and characterized to determine their mechanical properties, particularly Young's modulus, to be a close mechanical representative of skin and soft tissues. Young's modulus of soft tissues is rather low (in the kilopascal range) when examined at the macroscale of mass tissue assemblies, as being governed by the elastic stiffness of the extracellular matrix proteins (Akhtar et al., 2011). The stress-strain relation for different phantom concentrations is shown in Figure 10A, which demonstrated linearity up to 0.25 mm/mm strain. While increasing the compressive strain, the compressive stress increased, reaching higher values with higher gelatin concentrations. Subsequently, this led to a linear increase in the mean Young's modulus with the increase in gelatin concentration (Figure 10B).

4 Discussion

In this work, we utilized high-resolution acoustic mapping to plot the attenuation of ultrasound waves—at different frequencies, voltages, and duty cycles - as they travel through degassed water and soft tissue-mimicking gelatin phantoms. An acoustic assessment was performed by recording the intensity drop and lost power per unit area at the focal point of the three transducers and throughout the whole horizontal midplane scanned. The expected lifetime of each phantom depended on the percentage of gelatin concentration, whereby only the horizontal midplane was scanned to ensure that the phantoms were not submerged in water for a long period, thus avoiding any swelling or thinning out which would then affect the

10.3389/fbioe.2024.1276143

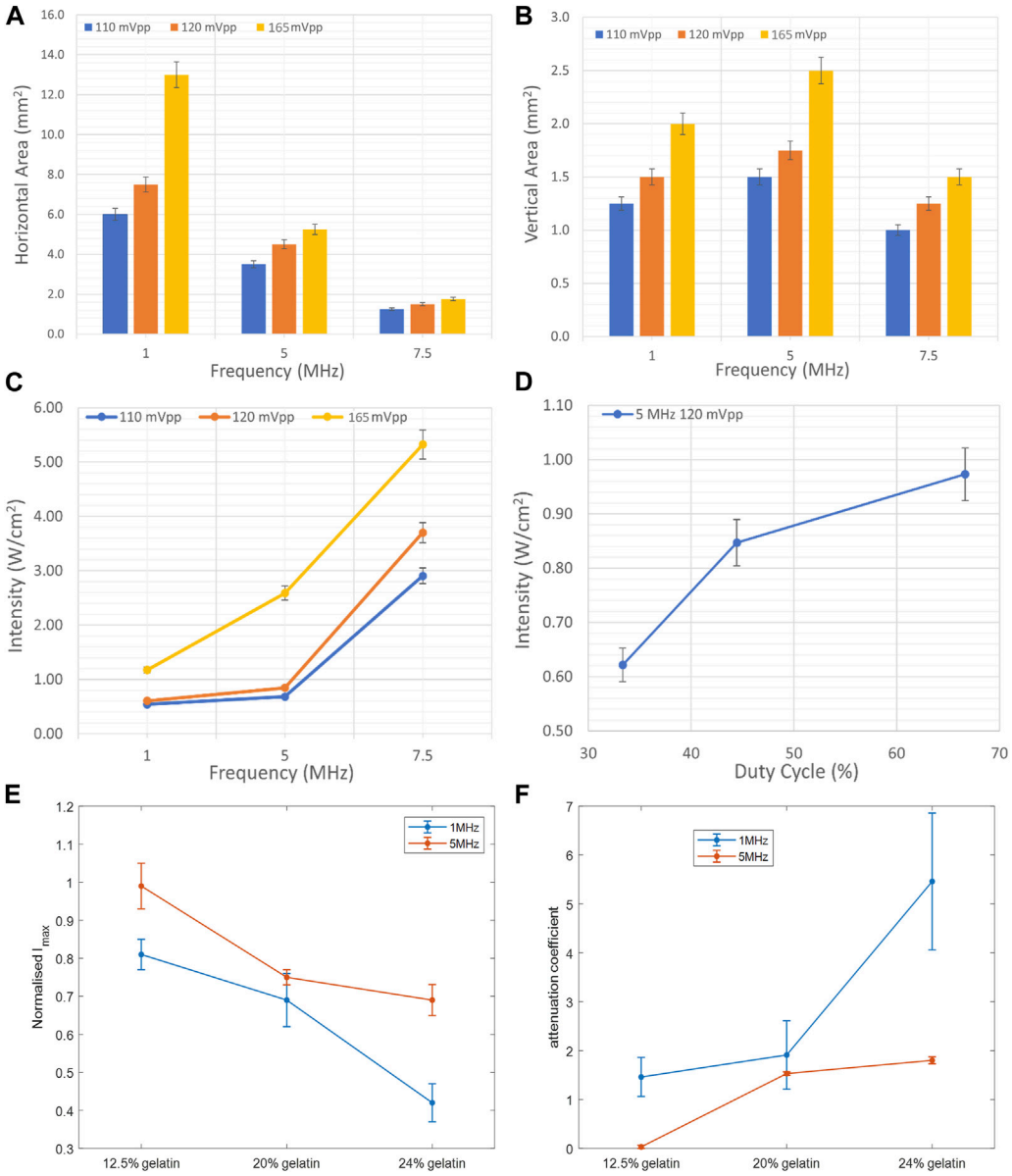

FIGURE 7
Effect of frequency, duty cycle, and gelatin concentration on the focal area and acoustic intensity. **(A)** Variation of the horizontal area at the horizontal midplane as a function of ultrasound frequency and voltage. **(B)** Variation of the area at the vertical cross section at the focal point as a function of ultrasound frequency and voltage. **(C)** Increase in the maximal intensity at the focal region as a function of increasing acoustic frequency and voltage. **(D)** Increase in the maximal intensity at the focal region as a function of increased duty cycle with the 5 MHz transducer at a voltage of 120 mV. Variation of the normalized maximal intensity **(E)** and attenuation coefficient **(F)** as a function of gelatin concentration, recorded while using the 1 MHz frequency and 5 MHz frequency transducers.

intensity measurements. Scanning one plane lasted for 1 h. Measuring the mass of the gelatin-based phantom before and after scanning the midplane showed no significant change in its mass. For an enhanced understanding of the acoustic attenuation of ultrasound waves propagating through the tissue-mimicking phantoms, we modeled the acoustic setup and ran simulations for outcome prediction and result validation. Whereas the mechanical assessment of the phantoms was estimated by measuring the variation in Young's modulus as a function of increasing gelatin concentrations. The compressive stress and strain were measured to study the elastic properties of the gelatin-based phantoms.

4.1 Acoustic profile assessment

To study the acoustic profiles of ultrasound transducers with different carrier frequencies, we designed a synchronized semi-automated system that scanned the volume in which ultrasound waves propagated and then processed the data in the form of heatmaps. The focal region of focused ultrasonic transducers was directly related to the operating frequency of the probe, showing a narrowing of the acoustic beam and focal region with the rise in carrier frequency (Zhao and Kim, 2018). Extending the "on time" of ultrasound delivery by increasing the duty cycle recorded higher

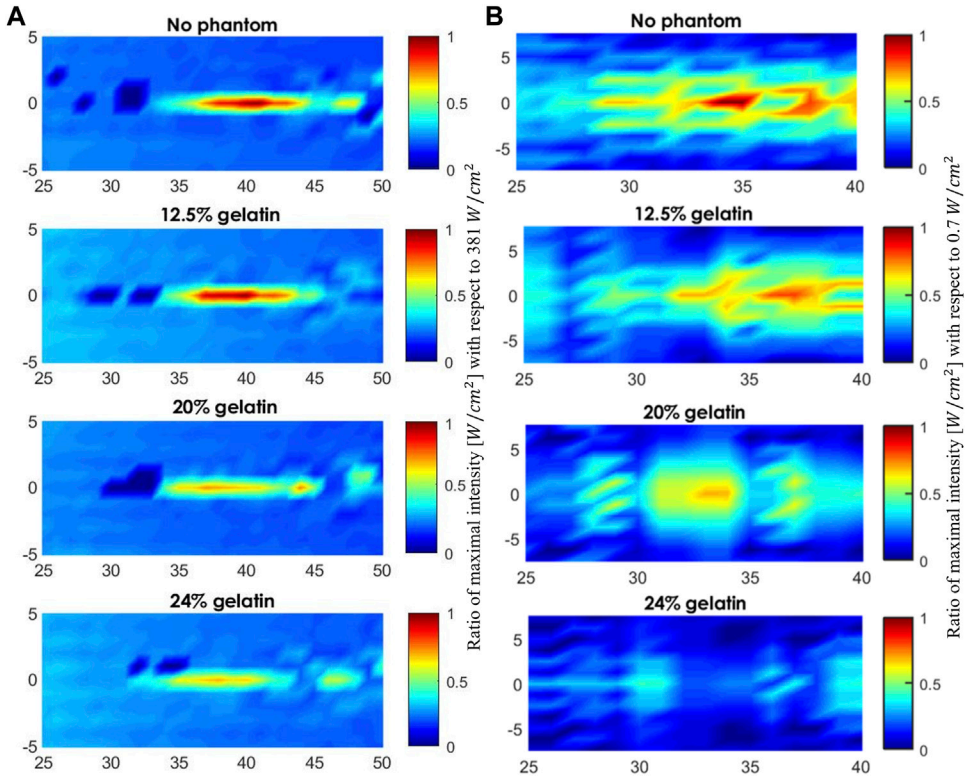

FIGURE 8
Acoustic profile of the mid-horizontal plane in front of the face of the transducer. **(A)** The scanned volume without a phantom placed and when the 12.5%, 20%, and 24% gelatin-based phantoms were positioned in place respectively using the 5 MHz transducer **(A)** and using the 1 MHz transducer **(B)**. The acoustic profiles display the maximal intensities plotted as a function of the maximal intensity recorded in water for visual inspection of the drop in intensity.

values of acoustic intensities and similar acoustic profiles. For a more confined acoustic profile spread and a higher acoustic intensity reached at the focal point, the 7.5 MHz transducer with a voltage range of 165 mV and ultrasound duty cycle of 67% achieved the desired results. However, higher frequencies could cause temperature rise when directed towards tissue-mimicking phantoms (Kaczmarek et al., 2018). Decreasing the carrier frequency of the ultrasound transducer allowed more penetrability and a wider acoustic profile spreading across the focal region.

Studying the acoustic properties of the prepared gelatin-based phantoms is essential for tissue-mimicking in ultrasound applications. The acoustic attenuation occurring at the focal point in particular, and the power and energy lost due to mechanical waves in general can help give a clearer idea of the percentage of intensity drop taking place in the tissue. Whether for ultrasound imaging purposes or ultrasound therapies, non-invasive techniques require optimal use of ultrasound parameters to ensure desirable results (Blackmore et al., 2019). The increase in the normalized intensity with respect to the maximal intensity recorded at the focal region when increasing the frequency of ultrasound from 1 MHz to 5 MHz emphasized the results of section 3.1.1 (Figures 7E,F). Whereby, in a given medium with a fixed voltage and ultrasound duty cycle, the 5 MHz ultrasound waves transferred more power per unit area. As the gelatin concentration increased, normalized intensities, with both ultrasound frequencies, went down due to less power transfer in a given unit of area as the molds got denser.

Furthermore, we designed a model to generate simulated data and compared it with our experimental results for prediction and validation purposes. The model examined the propagation of acoustic waves as they passed through the gelatin medium to the water medium. Following the variation in the speed of sound and medium density as in Table 1, the amplitude of the received signal at the focal point decreased and the spread of energy was more confined. Gu et al. reported a drop in the amplitude and phase difference between the simulated homogeneous and heterogeneous media, mainly from the variation in sound speed, density, absorption, and non-linearity coefficients (Gu and Jing, 2018).

The acoustic field predictions and maximal intensity drop at the focal point with respect to those recorded when the different phantoms were placed, one after the other, showed accurate estimations with an acceptable percentage of model deviation (Figure 9A). The variation in the attenuation coefficient calculated between simulated and measured data highly depended on the thickness of the sample (Figure 9B). In the simulation experiments, a fixed thickness of 8 mm was used, while in the experiments of ultrasound waves travelling according to the transmission method, a slight difference in the thickness of the used phantom specimens was recorded. The volume scans including the phantoms clearly illustrated the reduction in the transfer of power per unit area, hence the drop in the intensity values

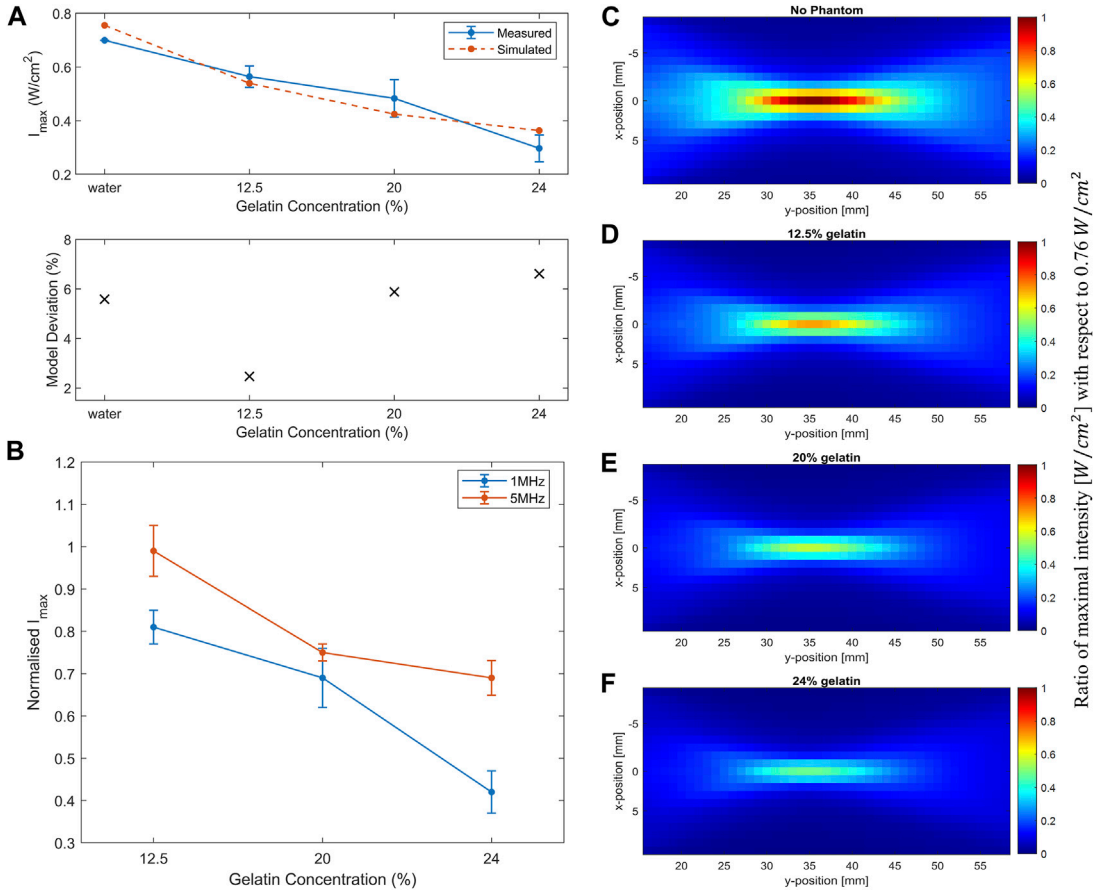

FIGURE 9
Simulation of acoustic wave propagation through different media. **(A)** Decrease in the simulated maximum intensity (dashed line) recorded at the focal point in water and as the gelatin concentration increased in comparison with the measured experimental maximal intensity (full line) while using the 1 MHz transducer. The deviation of simulated data from the measured data is less than 10%. **(B)** Increase in the attenuation coefficient α in the simulated (dashed line) and measured experimental data (full line) as a function of increased gelatin concentration. **(C)** Acoustic profile through water only with a maximum intensity of 0.76 W/cm^2 reached. **(D–F)** Visual representation of the acoustic profile where the phantoms with different gelatin concentrations (12.5%, 20% and 24%) were introduced respectively in front of the face of the 1 MHz transducer, showing the decrease in the maximal intensity recorded with respect to that calculated in the water-only medium.

throughout the horizontal plane. The structure, viscosity, and concentration of the gelatin gel affected its stress relaxation which caused higher acoustic attenuation and sensitivity to acoustic wave propagation (Parker and Povey, 2012). Taking the acoustic impedance into consideration, the values were within the same range of biological soft tissues, connective tissues and muscle (Culjat et al., 2010).

4.2 Mechanical assessment of phantom

Tissues have varying stiffness and elasticity levels ranging from the order of pascal (such as nerve cells and adipose tissues) to the order of Gigapascal (such as bones and tendons) (McKee et al., 2011). The mechanical properties of tissues differ depending on their heterogeneity at the microscale and macroscale as a result of their varied dimensions, shapes, and constituents. These properties have been outlined using the linear compressive Young's modulus for the quantification of tissue stiffness. In addition, the mechanical properties of tissue can be altered due to disease-enabling detection and diagnosis. For example, Hu et al. reported a mean Young's modulus of 66.4 ± 12.1 kPa in healthy thyroid nodules of patients while that of cancerous nodules was significantly lower, thus aiding with thyroid diagnosis (Hu et al., 2018). In addition, measurements of Young's modulus of breast tissues showed high dependence on the tissue precompression applied and tissue constituents, recording values ranging from a few kilopascals with normal tissues to folds higher with carcinomas and fibroglandular tissues (Samani et al., 2007; Ramiao et al., 2016).

In our work, the gelatin concentrations used mimicked the elasticity properties of such biological tissues (Figure 10C); whereby the mean Young's modulus estimated for each of the 12.5% and 20% phantom concentrations mimicked skin on the volar (101.180 kPa) and dorsal forearm (68.678 kPa) (Liang and Boppart, 2009) taking into consideration skin thickness measurements and the various skin layers at these sites; whereas the 24% phantom concentration mimicked the mechanical properties of a pre-stressed patella tendon (100.23 ± 44.61 kPa) (Kot et al., 2012) and certain skeletal muscles (120–170 kPa) (Guimarães et al., 2020). The range of gelatin percentages used

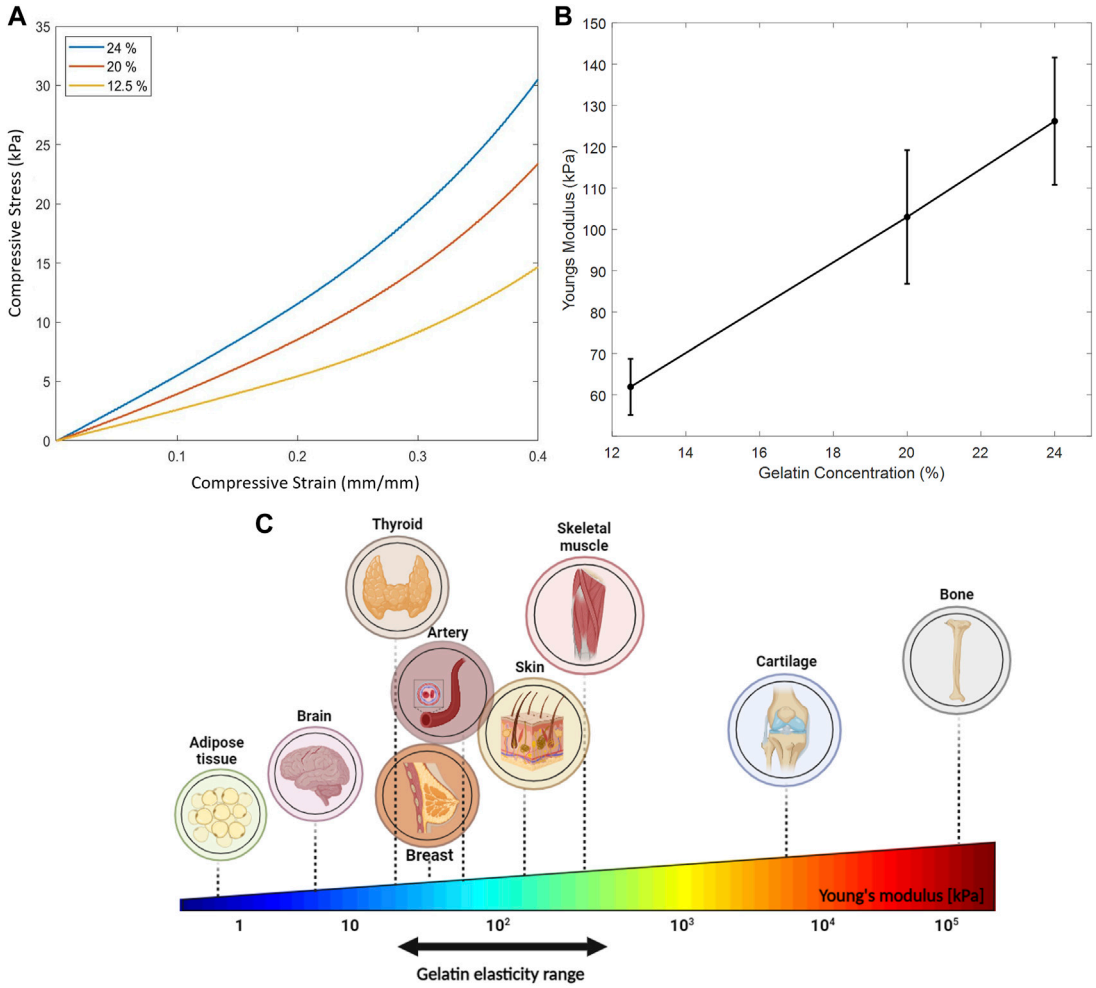

FIGURE 10
Mechanical properties of the gelatin-based phantoms. **(A)** Linear stress-strain relation up to 0.25 mm/mm strain of the three gelatin concentrations tested. **(B)** Increase in Young's modulus as a function of increasing gelatin concentration where 10 specimens of each concentration were tested. **(C)** Young's elasticity modulus of some biological tissues. Gelatin elasticity range of the three different gelatin concentrations used in our mechanical compression experiments mimic the stiffness of some biological tissues.

for this study took into consideration the following: a gelatin concentration lower than 12.5% caused the disintegration of the gelatin molds when submerged in water for a long period, thus tampering with the integrity of the results. Also, increasing the gelatin concentration beyond 24% risked mixture saturation and heterogeneity (Dahmani et al., 2019).

Mechanical testing demonstrated a rise in the elastic modulus with the addition of more gelatin powder to the solution. This could be a result of denser molds having higher stiffness and firmness after refrigeration. The variability in Young's moduli of the samples recorded experimentally could be a consequence of slight dehydration, as the sample phantoms were removed from the fridge, unmolded and specimens were cut out from them; Kalra et al. reported a significant reduction in Young's modulus of the outermost skin layer as a function of increased hydration (Kalra et al., 2016), thus affecting the skin's mechanical properties. In Figure 10A, and for the same stress applied, a smaller strain was recorded with higher gelatin concentrations; whereby adding more gelatin powder rendered the phantoms denser and more capable of withstanding compressive deformations in the direction of the applied force.

When mechanically assessing the phantoms, it should be noted that specimens obtained from the edges of the prepared gelatin molds recorded higher stiffness values than those cut out from the center, given that gelatin hardens faster at the surface and boundaries than in the middle areas. Humidity index and room temperature could also increase the degree of variability in gelatin properties, as well as increasing the gelatin concentration which makes the specimens denser and less homogeneous. It should be noted that the phantoms could only withstand being submerged in water for a certain period. Extended submergence caused the phantom to thin out at specific regions, impacting the reliability of the results. While gelatin-based phantoms are commonly used in ultrasound research due to their tunable mechanical properties, they may not fully replicate the diversity of human tissues in terms of density and geometric complexity, including interfaces between different tissues, blood vessels, and organ shapes (Chen et al., 2016). Add to that, our phantoms solely represented linear elastic

properties, overlooking the prevalent viscoelastic nature exhibited by most biological tissues. To address this, it is imperative to blend gelatin with other materials to encompass a wider range of control over the phantom's elastic behaviors.

The employed thermocouple featured a low acquisition frequency, and a maximum temperature detection limit of 120°C. Employing a smaller, more sensitive thermocouple with a broader detection range would yield superior results. Furthermore, manually positioning the thermocouple at the center of the transducer's focal area, where temperature variations are most pronounced, introduced an error in the data collection process. Our work offered a novel approach to cancer spheroid ablation within Matrigel, with a focus on avoiding high temperatures that could potentially harm healthy cells in future clinical applications. However, variations in spheroid sizes within the same petri dish posed challenges in studying the influence of HIFU parameters on spheroid dimensions and the inability to count cells prior to sonication hindered precise analysis.

5 Conclusion

In this work, we developed gelatin-based ultrasound phantoms of soft tissue and characterized them mechanically via unconfined compression tests, and acoustically via high-resolution acoustic mappings. We subsequently validated the results against acoustic simulations. High-resolution acoustic maps of the intensity distribution of ultrasound can provide essential information on the spatial changes in ultrasound wave intensity and focal point, enabling a more in-depth examination of the effect of tissue on acoustic waves. Our work described the acoustic and mechanical characterizations of a phantom suitable for investigating the effective intensity of an ultrasonic wave traversing soft tissues.

Examining the ultrasound intensity drops as a function of increased tissue elasticity and stiffness, mimicked by artificial *in vitro* phantoms, provided insight into the acoustic attenuations of ultrasound through. As ultrasonic waves transition between different media, the magnitude of energy loss increases. Estimation of the latter enhances pre-clinical and clinical works that employ ultrasound technology, whereby acoustic phantoms provide a safe and reliable way to study the behavior of sound waves and test the accuracy of acoustic measurements to evaluate the performance of acoustic devices.

Acquiring and maintaining physical tissue-mimicking phantoms can be costly, as they require materials, resources, and regular maintenance. However, simulating phantoms using computational models is often more cost-effective and accessible, allowing versatility, rapid prototyping and more controlled experimental settings. Advances in computational simulations of the acoustic profiles facilitate the prediction and validation of experimental outcomes for better results. For further enhancements and more precise measurements, the phantoms could be fabricated in more accurate geometrical shapes, specific to the tissue in concern. Henceforth, this work presented a reproducible method by which gelatin, a readily available material, could be characterized to mimic properties of soft tissues, using a motorized system to obtain high-resolution acoustic profiles of the traveling ultrasonic waves in characterized media.

Data availability statement

The raw data supporting the conclusion of this article will be made available by the authors, without undue reservation.

Author contributions

HB: Investigation, Writing–review and editing, Data curation, Formal Analysis, Methodology, Project administration, Writing–original draft. PR: Investigation, Methodology, Writing–review and editing. MK: Investigation, Writing–review and editing, Conceptualization.

Funding

The author(s) declare that no financial support was received for the research, authorship, and/or publication of this article.

Conflict of interest

The authors declare that the research was conducted in the absence of any commercial or financial relationships that could be construed as a potential conflict of interest.

Publisher's note

Supplementary material

The Supplementary Material for this article can be found online at: https://www.frontiersin.org/articles/10.3389/fbioe.2024.1276143/full#supplementary-material

Reference

Akhtar, R., Sherratt, M. J., Cruickshank, J. K., and Derby, B. (2011). Characterizing the elastic properties of tissues. *Mater. Today* 14 (3), 96–105. doi:10.1016/s1369-7021(11)70059-1

Baek, H., Pahk, K. J., and Kim, H. (2017). A review of low-intensity focused ultrasound for neuromodulation. *Biomed. Eng. Lett.* 7, 135–142. doi:10.1007/s13534-016-0007-y

Blackmore, J., Shrivastava, S., Sallet, J., Butler, C. R., and Cleveland, R. O. (2019). Ultrasound neuromodulation: a review of results, mechanisms and safety. *Ultrasound Med. Biol.* 45 (7), 1509–1536. doi:10.1016/j.ultrasmedbio.2018.12.015

Chen, A. I., Balter, M. L., Chen, M. I., Gross, D., Alam, S. K., Maguire, T. J., et al. (2016). Multilayered tissue mimicking skin and vessel phantoms with tunable mechanical, optical, and acoustic properties. *Med. Phys.* 43 (6Part1), 3117–3131. doi:10.1118/1.4951729

Chu, K. C., and Rutt, B. K. (1997). Polyvinyl alcohol cryogel: an ideal phantom material for MR studies of arterial flow and elasticity. *Magnetic Reson. Med.* 37 (2), 314–319. doi:10.1002/mrm.1910370230

Cook, J. R., Bouchard, R. R., and Emelianov, S. Y. (2011). Tissue-mimicking phantoms for photoacoustic and ultrasonic imaging. *Biomed. Opt. express* 2 (11), 3193–3206. doi:10.1364/boe.2.003193

Culjat, M. O., Goldenberg, D., Tewari, P., and Singh, R. S. (2010). A review of tissue substitutes for ultrasound imaging. *Ultrasound Med. Biol.* 36 (6), 861–873. doi:10.1016/j.ultrasmedbio.2010.02.012

Dahmani, J., Laporte, C., Pereira, D., Bélanger, P., and Petit, Y. (2019). Predictive model for designing soft-tissue mimicking ultrasound phantoms with adjustable elasticity. *IEEE Trans. Ultrasonics, Ferroelectr. Freq. Control* 67 (4), 715–726. doi:10.1109/tuffc.2019.2953190

Ebbini, E. S., and Ter Haar, G. (2015). Ultrasound-guided therapeutic focused ultrasound: current status and future directions. *Int. J. Hyperth.* 31 (2), 77–89. doi:10.3109/02656736.2014.995238

El Hassan, R., Lawand, N., Al-Chaer, E., and Khraiche, M. (2022). Frequency dependent, reversible focused ultrasound suppression of evoked potentials in the reflex arc in an anesthetized animal. *J. Peripher. Nerv. Syst.* 27 (4), 271–282. doi:10.1111/jns.12512

Escoffre, J.-M., and Bouakaz, A. (2015). *Therapeutic ultrasound*. Springer.

Food and Drug Administration (2008). *Guidance for industry and FDA staff information for manufacturers seeking marketing clearance of diagnostic ultrasound systems and transducers*. Rockville, MD: FDA.

Fromageau, J., Brusseau, E., Vray, D., Gimenez, G., and Delachartre, P. (2003). Characterization of PVA cryogel for intravascular ultrasound elasticity imaging. *IEEE Trans. ultrasonics, Ferroelectr. Freq. control* 50 (10), 1318–1324. doi:10.1109/tuffc.2003.1244748

Gu, J., and Jing, Y. (2018). Numerical modeling of ultrasound propagation in weakly heterogeneous media using a mixed-domain method. *IEEE Trans. ultrasonics, Ferroelectr. Freq. control* 65 (7), 1258–1267. doi:10.1109/tuffc.2018.2828316

Guimarães, C. F., Gasperini, L., Marques, A. P., and Reis, R. L. (2020). The stiffness of living tissues and its implications for tissue engineering. *Nat. Rev. Mater.* 5 (5), 351–370. doi:10.1038/s41578-019-0169-1

Hofstetter, L. W., Fausett, L., Mueller, A., Odéen, H., Payne, A., Christensen, D. A., et al. (2020). Development and characterization of a tissue mimicking psyllium husk gelatin phantom for ultrasound and magnetic resonance imaging. *Int. J. Hyperth.* 37 (1), 283–290. doi:10.1080/02656736.2020.1739345

Hu, L., He, N., Ye, L., Zhou, H., Zhong, W., and Zhang, X. (2018). Evaluation of the stiffness of tissues surrounding thyroid nodules with shear wave elastography. *J. Ultrasound Med.* 37 (9), 2251–2261. doi:10.1002/jum.14578

Kaczmarek, K., Hornowski, T., Kubovcikova, M., Timko, M., Koralewski, M., and Józefczak, A. (2018). Heating induced by therapeutic ultrasound in the presence of magnetic nanoparticles. *ACS Appl. Mater. interfaces* 10 (14), 11554–11564. doi:10.1021/acsami.8b02496

Kalra, A., Lowe, A., and Jumaily, A. A. (2016). An overview of factors affecting the skins Youngs modulus. *J. Aging Sci.* 4 (2), 1000156. doi:10.4172/2329-8847.1000156

Kamimura, H. A., Saharkhiz, N., Lee, S. A., and Konofagou, E. E. (2021). Synchronous temperature variation monitoring during ultrasound imaging and/or treatment pulse application: a phantom study. *IEEE open J. ultrasonics, Ferroelectr. Freq. control* 1, 1–10. doi:10.1109/ojuffc.2021.3085539

Kawabata, K. I., Waki, Y., Matsumura, T., and Umemura, S.-I. (2004). "Tissue mimicking phantom for ultrasonic elastography with finely adjustable elastic and echographic properties," in IEEE Ultrasonics Symposium, 2004, Montreal, Quebec, Canada, 23-27 August 2004 (IEEE).

Khraiche, M. L., El Emam, S., Akinin, A., Cauwenberghs, G., Freeman, W., and Silva, G. A. (2013). Visual evoked potential characterization of rabbit animal model for retinal prosthesis research. *Annu. Int. Conf. IEEE Eng. Med. Biol. Soc.* 2013, 3539–3542. doi:10.1109/EMBC.2013.6610306

Khraiche, M. L., and El Hassan, R. (2020). Advances in three-dimensional nanostructures for intracellular recordings from electrogenic cells. *J. Sci. Adv. Mater. Devices* 5 (3), 279–294. doi:10.1016/j.jsamd.2020.07.003

Khraiche, M. L., Jackson, N., and Muthuswamy, J. (2009). Early onset of electrical activity in developing neurons cultured on carbon nanotube immobilized microelectrodes. *Annu. Int. Conf. IEEE Eng. Med. Biol. Soc.* 2009, 777–780. doi:10.1109/IEMBS.2009.5333590

Khraiche, M. L., Phillips, W. B., Jackson, N., and Muthuswamy, J. (2008). Ultrasound induced increase in excitability of single neurons. *Annu. Int. Conf. IEEE Eng. Med. Biol. Soc.* 2008, 4246–4249. doi:10.1109/IEMBS.2008.4650147

Kim, J., Kim, M., Park, Y., and Ha, K. (2012). Acoustic characteristics of a tissue mimicking phantom for visualization of thermal distribution. *Jpn. J. Appl. Phys.* 51 (7S), 07GB10. doi:10.1143/jjap.51.07gb10

Kot, B. C. W., Zhang, Z. J., Lee, A. W. C., Leung, V. Y. F., and Fu, S. N. (2012). Elastic modulus of muscle and tendon with shear wave ultrasound elastography: variations with different technical settings. *PLoS One* 7, e44348. doi:10.1371/journal.pone.0044348

Kumar, K., Andrews, M. E., Jayashankar, V., Mishra, A. K., and Suresh, S. (2010). Measurement of viscoelastic properties of polyacrylamide-based tissue-mimicking phantoms for ultrasound elastography applications. *IEEE Trans. Instrum. Meas.* 59 (5), 1224–1232. doi:10.1109/tim.2009.2038002

Liang, X., and Boppart, S. A. (2009). Biomechanical properties of *in vivo* human skin from dynamic optical coherence elastography. *IEEE Trans. Biomed. Eng.* 57 (4), 953–959. doi:10.1109/TBME.2009.2033464

Madsen, E. L., Hobson, M. A., Shi, H., Varghese, T., and Frank, G. R. (2006). Stability of heterogeneous elastography phantoms made from oil dispersions in aqueous gels. *Ultrasound Med. Biol.* 32 (2), 261–270. doi:10.1016/j.ultrasmedbio.2005.10.009

Mahesh, M. (2013). The essential physics of medical imaging, third edition. *Med. Phys.* 40 (7), 077301. doi:10.1118/1.4811156

Maloney, E., and Hwang, J. H. (2015). Emerging HIFU applications in cancer therapy. *Int. J. Hyperth.* 31 (3), 302–309. doi:10.3109/02656736.2014.969789

Martin, E., Jaros, J., and Treeby, B. E. (2019). Experimental validation of k-wave: nonlinear wave propagation in layered, absorbing fluid media. *IEEE Trans. ultrasonics, Ferroelectr. Freq. control* 67 (1), 81–91. doi:10.1109/tuffc.2019.2941795

McKee, C. T., Last, J. A., Russell, P., and Murphy, C. J. (2011). Indentation versus tensile measurements of Young's modulus for soft biological tissues. *Tissue Eng. Part B Rev.* 17 (3), 155–164. doi:10.1089/ten.teb.2010.0520

Minton, J. A., Iravani, A., and Yousefi, A. M. (2012). Improving the homogeneity of tissue-mimicking cryogel phantoms for medical imaging. *Med. Phys.* 39 (11), 6796–6807. doi:10.1118/1.4757617

Negussie, A. H., Partanen, A., Mikhail, A. S., Xu, S., Abi-Jaoudeh, N., Maruvada, S., et al. (2016). Thermochromic tissue-mimicking phantom for optimisation of thermal tumour ablation. *Int. J. Hyperth.* 32 (3), 239–243. doi:10.3109/02656736.2016.1145745

Parker, N., and Povey, M. (2012). Ultrasonic study of the gelation of gelatin: phase diagram, hysteresis and kinetics. *Food Hydrocoll.* 26 (1), 99–107. doi:10.1016/j.foodhyd.2011.04.016

Polanía, R., Nitsche, M. A., and Ruff, C. C. (2018). Studying and modifying brain function with non-invasive brain stimulation. *Nat. Neurosci.* 21 (2), 174–187. doi:10.1038/s41593-017-0054-4

Prince, J. L., and Links, J. M. (2006). *Medical imaging signals and systems*. Upper Saddle River: Pearson Prentice Hall.

Ramiao, N. G., Martins, P. S., Rynkevic, R., Fernandes, A. A., Barroso, M., and Santos, D. C. (2016). Biomechanical properties of breast tissue, a state-of-the-art review. *Biomechanics Model. Mechanobiol.* 15, 1307–1323. doi:10.1007/s10237-016-0763-8

Samani, A., Zubovits, J., and Plewes, D. (2007). Elastic moduli of normal and pathological human breast tissues: an inversion-technique-based investigation of 169 samples. *Phys. Med. Biol.* 52 (6), 1565–1576. doi:10.1088/0031-9155/52/6/002

Takagi, R., Yoshinaka, K., Washio, T., and Koseki, Y. (2022). A visualization method for a wide range of rising temperature induced by high-intensity focused ultrasound using a tissue-mimicking phantom. *Int. J. Hyperth.* 39 (1), 22–33. doi:10.1080/02656736.2021.2012603

Treeby, B. E., and Cox, B. T. (2010). k-Wave: MATLAB toolbox for the simulation and reconstruction of photoacoustic wave fields. *J. Biomed. Opt.* 15 (2), 021314. doi:10.1117/1.3360308

Wang, Y., Tai, B. L., Yu, H., and Shih, A. J. (2014). Silicone-based tissue-mimicking phantom for needle insertion simulation. *J. Med. Devices* 8 (2), 021001. doi:10.1115/1.4026508

Wells, P. N., and Liang, H.-D. (2011). Medical ultrasound: imaging of soft tissue strain and elasticity. *J. R. Soc. Interface* 8 (64), 1521–1549. doi:10.1098/rsif.2011.0054

Yuan, Y., Wyatt, C., Maccarini, P., Stauffer, P., Craciunescu, O., MacFall, J., et al. (2012). A heterogeneous human tissue mimicking phantom for RF heating and MRI thermal monitoring verification. *Phys. Med. Biol.* 57 (7), 2021–2037. doi:10.1088/0031-9155/57/7/2021

Zarrintaj, P., Manouchehri, S., Ahmadi, Z., Saeb, M. R., Urbanska, A. M., Kaplan, D. L., et al. (2018). Agarose-based biomaterials for tissue engineering. *Carbohydr. Polym.* 187, 66–84. doi:10.1016/j.carbpol.2018.01.060

Zhao, L., and Kim, E. S. (2018). "Focused ultrasound transducer with electrically controllable focal length," in 2018 IEEE Micro Electro Mechanical Systems (MEMS), Belfast, UK, 21-25 January 2018 (IEEE).

Zhong, X., Zhou, P., Zhao, Y., Liu, W., and Zhang, X. (2022). A novel tissue-mimicking phantom for US/CT/MR-guided tumor puncture and thermal ablation. *Int. J. Hyperth.* 39 (1), 557–563. doi:10.1080/02656736.2022.2056249